Unsteady Transport of MHD Mixed Convection Inspired by Thermal Radiation and Partial Slip Performance: Finite Difference Approach

***Z. Iqbal*[a], *Ehtsham Azhar*[a,1], *Zaffar Mehmood*[a] *and Abid Kamran*[b]**

[a]Department of Mathematics, Faculty of Sciences, HITEC University, Taxila, Pakistan

[b]Capital University of Science and Technology Islamabad, Pakistan

Background: In this article mixed convection boundary layer flow of magneto-hydrodynamic (MHD) fluid on permeable stretching surface is investigated under the effects of velocity and thermal slip. The physical unsteady problem is examined by considering thermal radiation effects on momentum and thermal boundary layer flow. Different from available literature, in the present study we consider mix convective flow, thermal radiation, transverse applied magnetic field, velocity and thermal slip.
Methodology: The transform nonlinear system of differential equation is tackled numerically by the aid of finite difference scheme named as Keller-Box. Stable solution is correct up to six decimal places and special cases overlaps with the existing results in literature validating the present analysis.
Conclusion: It is concluded that mixed convection leads to accelerate fluid flow and reduce temperature profile. Injection contributes in rising magnitude of velocity and temperature when compared with suction effects. Velocity and thermal slip parameter influence in lowering fluid flow while temperature profile decrease for velocity slip parameter and opposite trend is witness corresponding to thermal slip parameter. Both velocity and temperature are increasing function of thermal radiation. In addition, the skin friction coefficient and the local Nusselt number are tabulated and analyzed.
Novelty: Present study is concerned with fluid flow applications in plastic films, polymer extrusion, glass fiber, metallurgical processes and metal spinning.
Keywords: *Finite difference; Computational design; Thermal and velocity slips; Thermal radiation.*

1. INTRODUCTION

The boundary layer flow over a stretching surface has a prominent place in engineering and industrial applications such as plastic films, polymer extrusion, glass fiber, metallurgical processes and metal spinning etc. In outlook of these practical aspects, Sakiadis [1] formulated boundary layer equation due to boundary layer flow over stretched surface. The stretching flows under various characteristics have been discussed extensively for steady flows (see [2-4]). The above studies are associated with stretching surfaces. However, flow over porous surfaces in steady flow has tremendous applications in filtration processes, metal and plastic extrusion, cosmic and geophysical sciences. Attia [5] examined heat transfer effects on a steady flow over a rotating disk in porous medium. Second law of thermodynamics is analyzed for steady flow of a nanofluid towards a rotating porous disk by Rashidi et al. [6]. Very recently, Manjunatha et al. [7] worked on conducting dusty fluid flow in porous medium towards stretching cylinder. They analyzed effect of curvature parameter on velocity and temperature distributions of fluid.
In practice, we rarely need to have a precise design of problems concerning with unsteady fluid flows. , Acharya et al. [8] analyzed effect of heat transfer of an unsteady flow over an infinite vertical porous

[1]Corresponding author:
E-mail address: ehtsham@uaar.edu.pk

plate. Similarly, water-gas flow influenced by heat transfer in porous medium is introduced by Gawin et al. [9]. Hayat et al. [10] carried out analysis on periodic MHD flows due to porous disk. An unsteady flow analysis is considered by Das et al. [11] in which mass transfer effects over moving porous plate is solved numerically. A non-Newtonian fluid induced by porous plate is studied by Hameed et al. [12]. Das et al. [13] investigated unsteady flow of a viscous fluid over a vertical porous plate with suction for constant magnetic field. Very recently, MHD rheological fluid flow over a porous medium is inspected by Nadeem et al. [14]. Unsteady dusty viscous flow of fluid submerged in parallel plates where upper plate is bounded by porous medium has been discussed by Parul and Manju [15]. They studied effect of magnetic field on flow velocity of both fluid and dust phase. Moreover, Sharma et al. [16] researched on influence of inclined magnetic field on an unsteady flow through porous media They proved that inclination cause a positive change in flow velocity and rate of shear stress at surface.

The MHD flow and thermal analysis in porous medium have become scorching issue for quite a long time, which is replicated in number of publications. Heat transfer and thermal radiation analysis is carried out on an unsteady mixed convection flow towards porous surface by Elbashbeshy and Aldawody [17]. Hayat et al. [18] found a series solution of mixed convection stagnation point flow over a porous medium under the influence of thermal radiation. Investigation of a micro polar fluid with radiation is considered by Rashidi and Abbasbandy [19]. Uwanta and Hamza [20] investigated time dependent convective flow between porous plates with thermal and suction/injection effects. The unsteady nanofluid flow is examined by Kandasamy and Muhaimin [21]. Hiemenznondarcy flow has been studied for magnetic field and thermal stratification induced by solar radiation over porous wedge. Introduction to heat exchanger efficiency over porous media is given by Shirvan et al. [22]. They gave a numerical solution which describes turbulent fluid flow. Some recent articles in this regard are cited ref. [23-25]

The aim of current study is to confer time-dependent MHD mixed convection flow with partial slip effects. In addition, thermal radiation effects are incorporated. Such analysis has concern with electric power generation, solar power technology, astrophysical flows, nuclear reactors, space vehicle re-entry and in other industrial areas. The presentation of present paper is as follows. Mathematical formulation is done in section 2. Sections 3 deal with numerical solutions and their convergence. Keller box method is used for computation of solution. Results and discussion are presented in section 4. Section 5 consists of main conclusions and novelty of present article.

2.PROBLEM FORMULATION AND GOVERNING EQUATIONS

We study MHD mixed convection flow of an incompressible viscous fluid bounded by a porous stretching sheet. The fluid is electrically conducting under time dependent magnetic field $B(t)$ exerted in a transverse influence of direction to flow. Induced magnetic field effect is absent whereas heat transfer is present in presence of thermal radiation. Moreover, sheet possesses velocity and thermal slip conditions. Here $x-$ and $y-$axes are selected parallel and perpendicular to the stretching sheet. Physical flow diagram and relevant coordinate system are incorporated in figure 1.

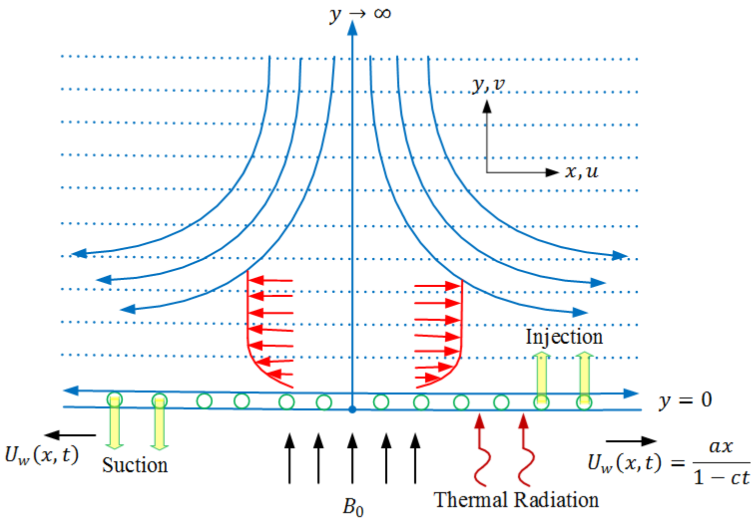

Fig. 1: Physical flow diagram and coordinate system

The governing equations of motion (i.e. the continuity, momentum, energy) in vector form for viscous fluid are as follow:

$$\nabla \cdot \bar{V} = 0, \tag{1}$$

$$\rho(\bar{V} \cdot \nabla)\bar{V} = k(\nabla \times \bar{N}) + m(T - T_\infty)\bar{g} + \mu\left(1 + \frac{1}{\beta} + k\right)\nabla^2\bar{V} - \frac{\mu}{k_1}\left(1 + \frac{1}{\beta}\right)\bar{V} - (\bar{J} \times \bar{B}), \tag{2}$$

$$\rho_j(\bar{V} \cdot \nabla)\bar{N} = k(\nabla \times \bar{V}) - 2k\bar{N} - \gamma(\nabla^2\bar{N}), \tag{3}$$

$$\bar{V} \cdot \nabla T = \alpha\nabla^2 T + \tau \cdot \nabla\bar{V} + \frac{1}{\rho C_p}(\bar{J} \times \bar{B}) \cdot \bar{V}, \tag{4}$$

$$\bar{V} \cdot \nabla C = D\nabla^2 C - k_1 C. \tag{5}$$

The component form of continuity, motion and energy equations provide

$$\frac{\partial u}{\partial x} + \frac{\partial v}{\partial y} = 0, \tag{6}$$

$$\frac{\partial u}{\partial t} + u\frac{\partial u}{\partial x} + v\frac{\partial u}{\partial y} = \nu\frac{\partial^2 u}{\partial y^2} - \frac{\sigma B^2(t)}{\rho}u + g\beta_T(T - T_\infty), \tag{7}$$

$$\rho c_p\left[\frac{\partial T}{\partial t} + u\frac{\partial T}{\partial x} + v\frac{\partial T}{\partial y}\right] = k\frac{\partial^2 T}{\partial y^2} - \frac{\partial q_r}{\partial y}, \tag{8}$$

in which u and v denote the velocity components in the x and $y -$ directions, respectively. ρ is the fluid density, ν is the kinematic viscosity, σ is the electrical conductivity, T is the temperature, c_p is the specific heat, k is the thermal conductivity of the fluid and q_r is the radiative heat flux.

In view of Rosseland approximation [17, 18], we can write

$$q_r = -\frac{4\sigma^*}{3k^*}\frac{\partial T^4}{\partial y}, \tag{9}$$

Where σ^* shows the Stefan-Boltzmann constant and k^* the mean absorption coefficient. Employing Taylor expansion and neglecting higher order terms we get

$$T^4 \approx 4T_\infty^3 T - 3T_\infty^4. \tag{10}$$

Hence Eqs. (8-10) give

$$\rho c_p\left[\frac{\partial T}{\partial t} + u\frac{\partial T}{\partial x} + v\frac{\partial T}{\partial y}\right] = \frac{\partial}{\partial y}\left[\left(\frac{16\sigma^* T_\infty^3}{3k^*} + k\right)\frac{\partial T}{\partial y}\right], \tag{11}$$

The appropriate boundary conditions are

$$u = U_w + N\mu \frac{\partial u}{\partial y}, \qquad v = V_w, \;\; T = T_w + K\frac{\partial T}{\partial y} \quad at\; y = 0, \tag{12}$$

$$u \to 0, T \to T_\infty \quad as \quad y \to \infty. \tag{13}$$

$$V_w = -\sqrt{\frac{\nu U_w}{x}}\, f(0). \tag{14}$$

Here indicates the mass transfer at surface with $V_w > 0$ for injection and $V_w < 0$ for suction, $N = N_0(1-ct)^{1/2}$ is slip factor, $K = K_0(1-ct)^{1/2}$ is thermal slip factor and for $N = 0 = K$, the no-slip conditions are recovered. The stretching velocity $U_w(x,t)$ and surface temperature $T_w(x,t)$ are taken as

$$U_w(x,t) = \frac{ax}{1-ct}, \quad T_w(x,t) = T_\infty + \frac{bx}{1-ct}, \tag{15}$$

where a, b and c denote the constants with $a > 0,\; b \geq 0$ and $c \geq 0$ and $(with\; ct < 1)$. Note that a and c have dimension of time^{-1}. Consider choosing $B(t) = B_0(1-ct)^{-1/2}$ with B_0as the uniform magnetic field and introducing

$$\eta = \sqrt{\frac{U_w}{\nu x}}\,y, \quad \psi = \sqrt{\nu x U_w}\, f(\eta), \qquad \theta(\eta) = \frac{T - T_\infty}{T_w - T_\infty}, \tag{16}$$

$$u = \frac{\partial \psi}{\partial y}, \;\; v = -\frac{\partial \psi}{\partial x}. \tag{17}$$

The continuity equation (6) identically satisfied and the resulting problems for f and θ are

$$f''' + ff'' - f'^2 - A^*\left(f' + \frac{1}{2}\eta f''\right) - M^2 f' + \lambda\theta = 0, \tag{18}$$

$$\frac{1}{Pr}\left(1 + \frac{4}{3N_r}\right)\theta'' + f\theta' - f'\theta - A^*\left(\theta + \frac{1}{2}\eta\theta'\right) = 0, \tag{19}$$

$$f(0) = S, \qquad f'(0) = 1 + S_f f''(0), \qquad f'(\eta) \to 0 \quad as \quad \eta \to \infty,$$
$$\theta(0) = 1 + S_T\theta'(0), \quad \theta(\eta) \to 0 \qquad as \quad \eta \to \infty. \tag{20}$$

Where ψ is the stream function, $f(0) = S$ (with $S < 0$ corresponds to suction and $S > 0$ shows injection), $A^* = \frac{c}{a}$ is unsteadiness parameter and for $A^* = 0$ the problems reduce to the steady state situation. The Hartman number M, Prandtl number Pr, the radiation parameter N_r, mixed convection parameter λ, the local Grashof number Gr_x, the non-dimensional slip factor S_f, and the non-dimensional thermal slip parameter S_T are defined by

$$M^2 = \frac{\sigma B_0^2}{a\rho}, \qquad Pr = \frac{\mu c_p}{k}, \qquad N_r = \frac{4\sigma^* T_\infty^3}{3k^* k}, \qquad \lambda = \frac{Gr_x}{Re_x^2}, \qquad Re_x = \frac{U_w x}{\nu},$$
$$Gr_x = \frac{g\beta(T_w - T_\infty)x^3/\nu^2}{U_w^2 x^2/\nu^2}, \;\; S_f = N_0\rho\sqrt{a\nu}, \quad S_T = K_0\sqrt{\frac{a}{\nu}}, \tag{21}$$

where prime is used for the differentiation with respect to η.

The skin friction coefficient C_f and local Nusselt number N_{u_x} are defined as

$$C_f = \frac{\tau_w}{\rho U_w^2/2}, \quad N_{u_x} = \frac{x q_w}{k(T_w - T_\infty)}, \tag{22}$$

where the skin friction τ_w and the heat transfer from the plate q_w are

$$\tau_w = \mu\left(\frac{\partial u}{\partial y}\right)\Bigg|_{y=0}, \quad q_w = -k\left(\frac{\partial T}{\partial y}\right)\Bigg|_{y=0}. \tag{23}$$

Dimensionless forms of Eq. (23) are

$$\frac{1}{2}C_f Re_x^{1/2} = f''(0), \qquad N_{u_x}/Re_x^{\frac{1}{2}} = -\theta'(0). \tag{24}$$

3. COMPUTATIONAL DESIGN

Keller box method is used to solve the nonlinear ordinary differential equations (18) and (19) subject to boundary conditions equation (20). This scheme is unconditionally stable and achieves exceptional accuracy. The complete flow chart of this implicit finite difference scheme is as follows:

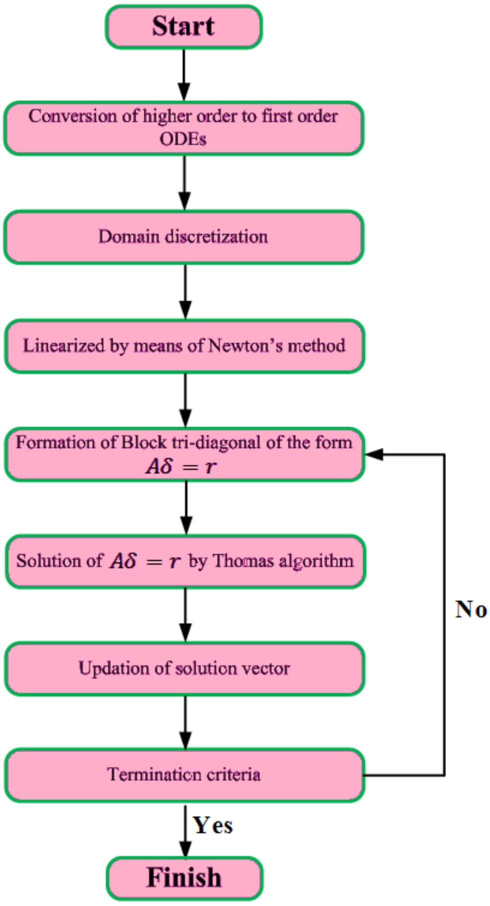

Keller box scheme flow chart

We start with introducing new independent variables$u(x,\ \eta)$, $v(x,\ \eta)$ and $t(x,\ \eta)$ with $f' = u$, $u' = v$ and$\theta' = t$, so that equations (18-19) reduces to first order form i.e.

$$v' + fv - u^2 - A^*\left(u + \frac{\eta}{2}v\right) - M^2 u + \lambda\theta = 0, \tag{25}$$

$$\left(1 + \frac{4}{3Nr}\right)t' + Prft - Pru\theta - A^*\left(\theta + \frac{\eta}{2}t\right) = 0. \tag{26}$$

The rectangular grid in $x - \eta$ plane is shown in Fig. 2 and net points are:

$$x^0 = 0, \quad x^i = x^{i-1} + k_i, \qquad i = 1,2, \dots, J,$$

$$\eta_0 = 0, \quad \eta_j = \eta_{j-1} + h_j, \qquad j = 1,2, \dots, J,$$

Where k_i and h_j are the Δx and $\Delta\eta$ −spacing. Here i and j are just sequences of numbers that indicate the coordinate location.

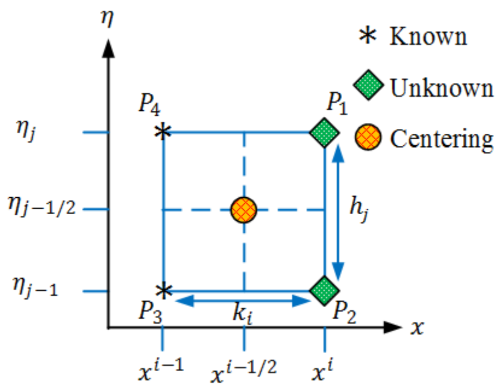

Fig. 2: Schematic representation of domain

Using central difference formulation at midpoint $\left(x^i, \eta_{j-\frac{1}{2}}\right)$ as

$$f_j^i - f_{j-1}^i - \frac{h_j}{2}\left(u_j^i + u_{j-1}^i\right) = 0, \tag{27}$$

$$u_j^i - u_{j-1}^i - \frac{h_j}{2}\left(v_j^i + v_{j-1}^i\right) = 0, \tag{28}$$

$$\theta_j^i - \theta_{j-1}^i - \frac{h_j}{2}\left(t_j^i + t_{j-1}^i\right) = 0, \tag{29}$$

Now applying central differencing, Eqs. (25) and (26) at point $\left(x^{i-1/2}, \eta_{j-\frac{1}{2}}\right)$

$$\left(v_j^i - v_{j-1}^i\right) + hf_{j-1/2}^i v_{j-1/2}^i - h\left(u_{j-1/2}^i\right)^2 - hA^*\left(u_{j-1/2}^i + \frac{\eta_{j-1/2}}{2} v_{j-1/2}^i\right) - hM^2 u_{j-1/2}^i + h\lambda\theta_{j-1/2}^i = R_{j-1/2}, \tag{30}$$

$$\left(1 + \frac{4}{3Nr}\right)\left(t_j^i - t_{j-1}^i\right) + hPrf_{j-1/2}^i t_{j-1/2}^i - hPru_{j-1/2}^i \theta_{j-1/2}^i - hA^*\left(\theta_{j-1/2}^i + \frac{\eta_{j-1/2}}{2} t_{j-1/2}^i\right) = T_{j-1/2}, \tag{31}$$

where $R_{j-1/2}$ and $T_{j-1/2}$ are known quantities i.e.

$$R_{j-1/2} = -\left(v_j^{i-1} - v_{j-1}^{i-1}\right) - hf_{j-1/2}^{i-1} v_{j-1/2}^{i-1} + h\left(u_{j-1/2}^{i-1}\right)^2 + hA^*\left(u_{j-1/2}^{i-1} + \frac{\eta_{j-1/2}}{2} v_{j-1/2}^{i-1}\right) + hM^2 u_{j-1/2}^{i-1} + h\lambda\theta_{j-1/2}^{i-1}, \tag{32}$$

$$T_{j-1/2} = -\left(1 + \frac{4}{3Nr}\right)\left(t_j^{i-1} - t_{j-1}^{i-1}\right) - hPrf_{j-1/2}^{i-1} t_{j-1/2}^{i-1} + hPru_{j-1/2}^{i-1}\theta_{j-1/2}^{i-1} + hA^*\left(\theta_{j-1/2}^{i-1} + \frac{\eta_{j-1/2}}{2} t_{j-1/2}^{i-1}\right). \tag{33}$$

and boundary condition reduce to

$$f_0^i = S,\ u_0^i = 1 + S_f v_0^i,\ u_J^i = 0,\ \theta_0^i = 1 + S_T t_0^i,\ \theta_J^i = 0. \tag{34}$$

Newton's method to linearize Eqs. (30-31), we introduce following iterates:

$$f_j^{(i+1)} = f_j^{(i)} + \delta f_j^{(i)},\ u_j^{(i+1)} = u_j^{(i)} + \delta u_j^{(i)},\ v_j^{(i+1)} = v_j^{(i)} + \delta v_j^{(i)},\ \theta_j^{(i+1)} = \theta_j^{(i)} + \delta\theta_j^{(i)}, t_j^{(i+1)} = t_j^{(i)} + \delta t_j^{(i)}. \tag{35}$$

Substituting above expressions in Eqs. (30-31) and then drop quadratic and higher order terms in $\delta f_j^{(i)},\ \delta u_j^{(i)},\ \delta v_j^{(i)},\ \delta\theta_j^{(i)},\ \delta t_j^{(i)},$ this procedure yields the following tridiagonal system

$$\delta f_j - \delta f_{j-1} - \frac{h_j}{2}\left(\delta u_j - \delta u_{j-1}\right) = (r_1)_j, \tag{36}$$

$$\delta u_j - \delta u_{j-1} - \frac{h_j}{2}\left(\delta v_j - \delta v_{j-1}\right) = (r_2)_j, \tag{37}$$

$$\delta\theta_j - \delta\theta_{j-1} - \frac{h_j}{2}\left(\delta t_j - \delta t_{j-1}\right) = (r_2)_j, \tag{38}$$

$$(a_1)_{j-1/2}\delta v_j + (a_2)_{j-1/2}\delta v_{j-1} + (a_3)_{j-1/2}\delta u_j + (a_4)_{j-1/2}\delta u_{j-1} + (a_5)_{j-1/2}\delta f_j +$$

$$(a_6)_{j-1/2}\delta f_{j-1} + (a_7)_{j-1/2}\delta\theta_j + (a_8)_{j-1/2}\delta\theta_{j-1} = (r_4)_{j-1/2}, \tag{39}$$

$$(b_1)_{j-1/2}\delta u_j + (b_2)_{j-1/2}\delta u_{j-1} + (b_3)_{j-1/2}\delta f_j + (b_4)_{j-1/2}\delta f_{j-1} + (b_5)_{j-1/2}\delta t_j + (b_6)_{j-1/2}\delta t_{j-1} + (b_7)_{j-1/2}\delta\theta_j + (b_8)_{j-1/2}\delta\theta_{j-1} = (r_5)_{j-1/2}, \tag{40}$$

In which

$$(a_1)_{j-1/2} = 1 + \frac{h_j}{4} f_{j-1/2} - \frac{h_j A^* \eta_{j-1/2}}{4} = (a_2)_{j-1/2} + 2, \tag{41}$$

$$(a_3)_{j-1/2} = -\frac{h_j}{2} u_{j-1/2} - \frac{h_j}{2}(A^* + M^2) = (a_4)_{j-\frac{1}{2}}, \tag{42}$$

$$(a_5)_{j-1/2} = \frac{h_j}{4} v_{j-1/2} = (a_6)_{j-1/2},\ (a_7)_{j-1/2} = \frac{h_j}{2}\lambda = (a_8)_{j-1/2}, \tag{43}$$

$$(b_1)_{j-1/2} = -\frac{h_j Pr}{2}\theta_{j-1/2} = (b_2)_{j-1/2},\ (b_3)_{j-1/2} = \frac{h_j Pr}{4} t_{j-1/2} = (b_4)_{j-1/2}, \tag{44}$$

$$(b_5)_{j-1/2} = \left(1 + \frac{4}{3Nr}\right) + \frac{h_j Pr}{4} f_{j-1/2} - \frac{h_j Pr A^* \eta_{j-1/2}}{4}, \tag{45}$$

$$(b_6)_{j-1/2} = -\left(1 + \frac{4}{3Nr}\right) + \frac{h_j Pr}{4} f_{j-1/2} - \frac{h_j Pr A^* \eta_{j-1/2}}{4}, \tag{46}$$

$$(b_7)_{j-1/2} = -\frac{h_j Pr}{4} u_{j-1/2} - \frac{h_j Pr A^*}{2} = (b_8)_{j-1/2}, \tag{47}$$

and

$$(r_4)_{j-1/2} = -(v_j - v_{j-1}) - h f_{j-1/2} v_{j-1/2} + h\left(u_{j-1/2}\right)^2 + hA^*\left(u_{j-1/2} + \frac{\eta_{j-1/2}}{2} v_{j-1/2}\right) + hM^2 u_{j-1/2} + h\lambda\theta_{j-1/2} + R_{j-1/2}, \tag{48}$$

$$(r_5)_{j-1/2} = -\left(1 + \frac{4}{3Nr}\right)(t_j - t_{j-1}) - hPr f_{j-1/2} t_{j-1/2} + hPr u_{j-1/2}\theta_{j-1/2} + hA^*\left(\theta_{j-1/2} + \frac{\eta_{j-1/2}}{2} t_{j-1/2}\right) + T_{j-1/2}. \tag{49}$$

Boundary condition becomes

$$\delta f_0 = 0,\ \delta u_0 = 0,\ \delta\theta_0 = 0,\ \delta u_J = 0,\ \delta\theta_J = 0. \tag{50}$$

Linearized difference equations (36-40) can be written in the block tridiagonal form, i.e.

$$\begin{bmatrix} [A_1] & [C_2] & & & \\ [B_2] & [A_2] & [C_2] & & \\ & \cdots & \cdots & & \\ & & [B_{J-1}] & [A_{J-1}] & [C_{J-1}] \\ & & & [B_J] & [A_J] \end{bmatrix} \begin{bmatrix} [\delta_1] \\ [\delta_2] \\ \cdots \\ [\delta_{J-1}] \\ [\delta_J] \end{bmatrix} = \begin{bmatrix} [r_1] \\ [r_2] \\ \cdots \\ [r_{J-1}] \\ [r_J] \end{bmatrix},$$

where elements are

$$[A_1] = \begin{bmatrix} 0 & 0 & 1 & 0 & 0 \\ -\frac{h}{2} & 0 & 0 & -\frac{h}{2} & 0 \\ 0 & -\frac{h}{2} & 0 & 0 & -\frac{h}{2} \\ (a_2)_1 & 0 & (a_5)_1 & (a_1)_1 & 0 \\ 0 & (b_6)_1 & (b_3)_1 & 0 & (b_5)_1 \end{bmatrix},$$

$$[A_J] = \begin{bmatrix} -\frac{h_j}{2} & 0 & 1 & 0 & 0 \\ -1 & 0 & 0 & -\frac{h_j}{2} & 0 \\ 0 & -1 & 0 & 0 & -\frac{h_j}{2} \\ (a_4)_j & 0 & (a_5)_1 & (a_1)_1 & 0 \\ (b_2)_j & (b_8)_j & (b_3)_j & 0 & (b_5)_j \end{bmatrix}, \quad 2 \le j \le J,$$

$$[B_J] = \begin{bmatrix} 0 & 0 & -1 & 0 & 0 \\ 0 & 0 & 0 & -\frac{h_j}{2} & 0 \\ 0 & 0 & 0 & 0 & -\frac{h_j}{2} \\ 0 & 0 & (a_6)_j & (a_2)_j & 0 \\ 0 & 0 & (b_4)_j & 0 & (b_6)_j \end{bmatrix}, \quad 2 \le j \le J,$$

$$[C_J] = \begin{bmatrix} -\frac{h_j}{2} & 0 & 0 & 0 & 0 \\ 1 & 0 & 0 & 0 & 0 \\ 0 & 1 & 0 & 0 & 0 \\ (a_3)_j & (a_7)_j & 0 & 0 & 0 \\ (b_1)_j & (b_7)_j & 0 & 0 & 0 \end{bmatrix}, \quad 2 \le j \le J.$$

By using LU method the block tridiagonal matrix is solved. Value of δ is calculated again and again until it satisfies the following condition:

$$\left|\delta v_0^{(i)} \le \epsilon_1,\right|$$

where $\epsilon_1 = 10^{-6}$ is small prescribed value.

4. THEORETICAL RESULTS AND DISCUSSION

This section is represented physical interpretation of predicted parameter on velocity and temperature profile. Blue lines are plotted against suction ($S < 0$) while Red lines represented the injection case ($S > 0$). The effects of mixed convection parameter λ on $f'(\eta)$ and $\theta(\eta)$ are shown in figure 3 and 4 respectively. As λ is directly related to buoyancy force this mean increasing values of mixed convection parameter yields stronger buoyancy force. Due to this velocity of the flow increases (see figure 3). This trend is more prominent for suction as compared to injection. Figure 4 depict that an opposite behavior is observed for temperature profile because when viscous boundary layer increases as a results thermal boundary layer decreases. Ratio of electromagnetic force to the viscous force is called Hartman number M which is plotted in figures 5 and 6 $f'(\eta)$ is a decreasing function of M due to the reason that increasing Hartman number lead to increase in electromagnetic force therefore magnitude of the velocity decrease (see figure 5). It is observed from figure 6 that temperature is an increasing function of M but this increase is more rapid for $S < 0$. The influence of unsteady parameter $A^*$is demonstrated from figure 7 and 8. Both velocity and temperature reduces with rising values of unsteady parameter also momentum and thermal boundary layer thickness decreases. The contribution of Prandtl number Pr on $f'(\eta)$ and $\theta(\eta)$ have been displayed in figures 9 and 10. Increase in Pr tends to enhancing momentum diffusivity. As a result velocity of the fluid and corresponding viscous boundary layer thickness decays (see figure 9). Whereas thermal diffusivity is inversely related to Prandtl number due to this fluid has a thinner thermal boundary layer which increases gradient of temperature and lowering $\theta(\eta)$as shown in figure 10. N_r being a radiation parameter is portrayed through figure 11 for velocity and figure 12 for temperature. Thermal conductivity is inversely proportional to N_r which contributes in up surging $f'(\eta)$ as represented in figure 11. Radiation parameter amplifies thermal capability of fluid flow. Hence temperature rises with thermal radiation parameterN_r. This information is demonstrated through Fig. 12 Influence of thermal slip parameter S_T and velocity slip parameter S_f are depicted through figures 13-16. From figures 13 and 14 confirms that velocity and temperature of the fluid decreases when thermal slip parameter rises. As by the definition of S_T kinematic viscosity of fluid decrease when thermal slip parameter increases due to which enhances viscous forces and lowering thermal forces.

Figures 15 and 16 are portrayed against S_f for $f'(\eta)$ and $\theta(\eta)$.It is observed that increases values of velocity slip parameter results a lowering fluid velocity and up surging temperature profile.
Check the accuracy and reliability of proposed method a comparative analysis of skin friction coefficient and local Nusselt number is presented through tables. Table 1shows relative investigation of $-f''(0)$ corresponding to S_f when $A^* = 0 = S = M$, and compared with the exact analytical solution [26]. The variation of heat transfer characteristic at the wall $-\theta'(0)$ when $M = S_T = S_f = 0 = N_r$ for different values of A^*, S, Pr is given in Table 2 and comparison with existing results also shown. We predict from this table that proposed technique having an excellent agreement with exact solution [27]. Table 3 presents values of $-\theta'(0)$ for some values of A^*, M, N_r when $Pr = 0.5 = S$, $S_f = 0.0 = S_T$. The magnitude of $-\theta'(0)$ decreases when M and N_r increase. However it increases for larger values of A^* Table 4 consists of the values of skin friction coefficient $\frac{1}{2}C_f Re_x^{1/2}$ and $-\theta'(0)$ for the parameters A^*, M, S and S_f when $Pr = 1.0$, $N_r = 0.2$ and $S_T = 0.1$. Numerical values of this table shows that skin friction coefficient enhances for rising values of M, S and A^* whereas it decays corresponding to S_f While local heat flux is decreasing function of M, S_f and opposite trend is witness for S, A^* Table 5 presents the values of $-\theta'(0)$for some values of Pr, N_r and S_T when $A^* = 0.2$, $S = 0.5$ and $S_f = 1.0$. It is obvious that magnitude of $-\theta'(0)$ increases for large values of Pr and decreases for rising values of S_T and N_r. Moreover, flow patterns are displayed in Fig. 17 for different values of A. It is evident that symmetry about vertical axis exists for flow pattern.

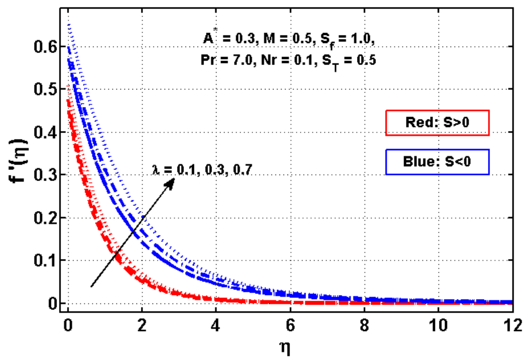

Fig. 3: Variation of λ on velocity

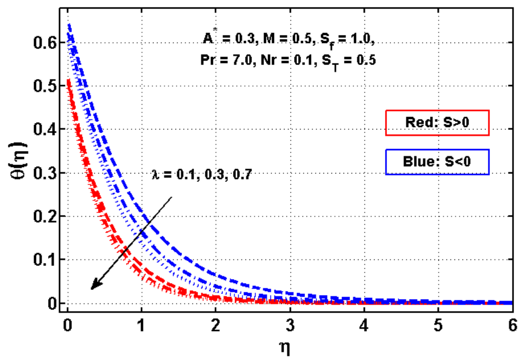

Fig. 4: Variation of λ on temperature

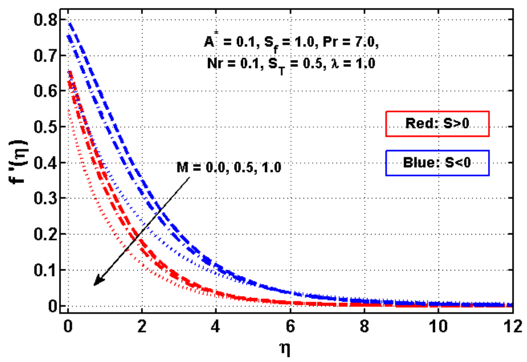

Fig. 5: Variation of M on velocity

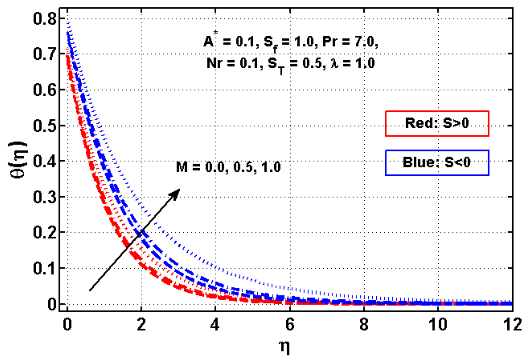

Fig. 6: Variation of M on temperature

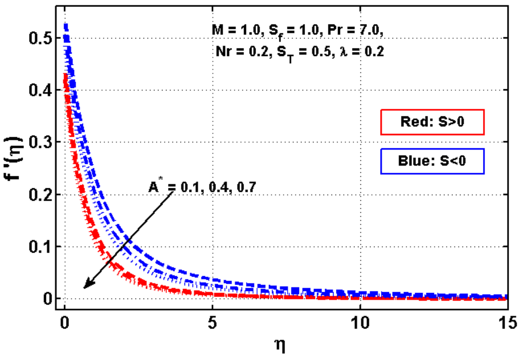

Fig. 7: Variation of A^* on velocity

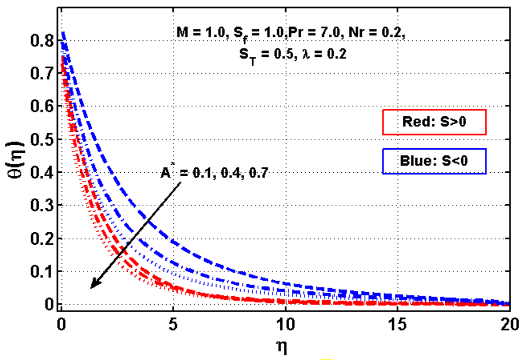

Fig. 8: Variation of A^* on temperature

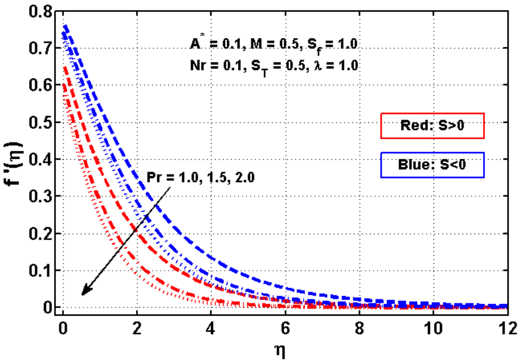

Fig. 9: Variation of Pr on velocity

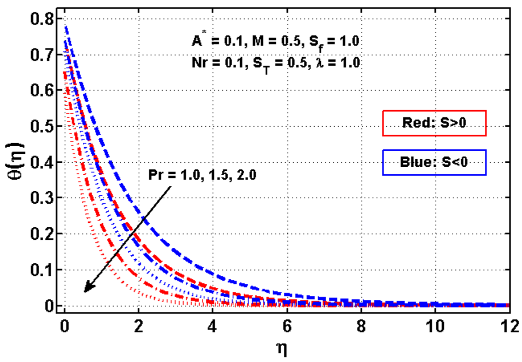

Fig. 10: Variation of Pr on temperature

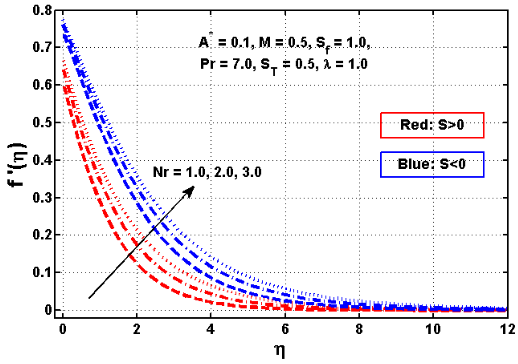

Fig. 11: Variation of Nr on velocity

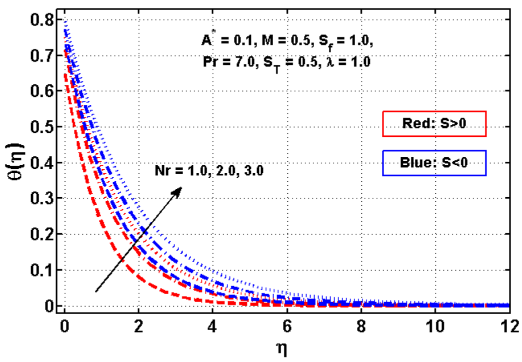

Fig. 12: Variation of Nr on temperature

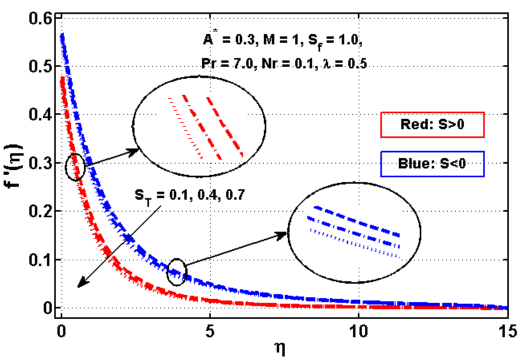

Fig. 13: Variation of S_T on velocity

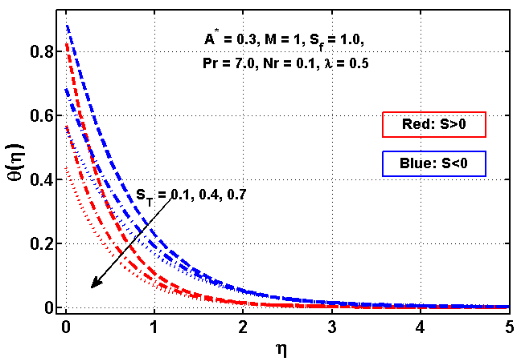

Fig. 14: Variation of S_T on temperature

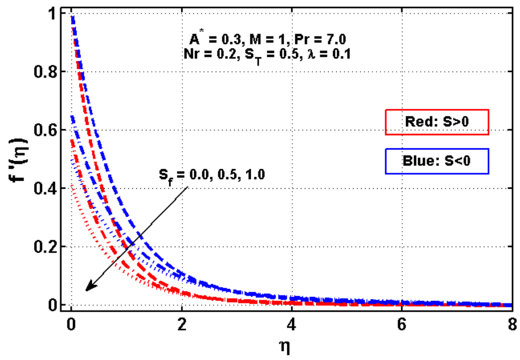

Fig. 15: Variation of S_f on velocity

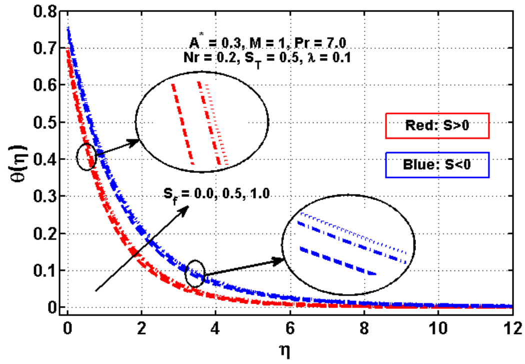

Fig. 16: Variation of S_f on temperature

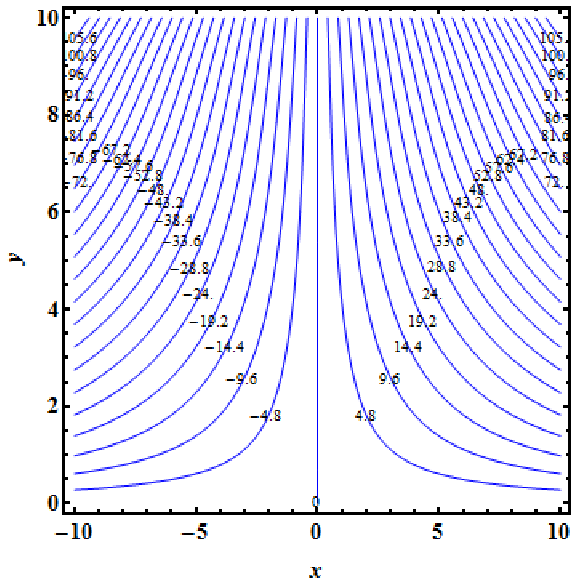

Fig. 17: Flow pattern for different values of A

Table 1 . Comparison of values of C_f with those of Wang [26] for various values of S_f when $A^* = S = M = \lambda = 0$.

S_f	Wang[26]	Finite difference approximation
0.0	1.0000	1.000000
0.1	0.8721	0.872082
0.2	0.7764	0.776377
0.5	0.5912	0.591195
1.0	0.4302	0.430162
2.0	0.2840	0.283981
5.0	0.1448	0.144841
10.0	0.0812	0.081249
20.0	0.0438	0.043782
50.0	0.0186	0.018634
100.0	0.0095	0.009581

Table 2 . Comparison of values of $-\theta'(0)$with those of Ishak et al. [27] for various values of A^*, S and Pr when $M = N_r = S_f = S_T = 0$.

A^*	S	Pr	Ishak et al. [27]	Finite difference approximation
0	−1.5	0.72	0.4570268	0.4570268

		1	0.5000000	0.5000000
		10	0.6541612	0.6541612
	0	0.72	0.8086313	0.8086313
		1	1.0000000	1.0000000
		3	1.9236825	1.9236825
		10	3.7206739	3.7206739
	1.5	0.72	1.4943684	1.4943684
		1	2.0000000	2.0000000
		10	16.084218	16.084218
1	−1.5	1	0.8095484	0.8095484
	0		1.3205534	1.3205534
	2		2.2223486	2.2223486

Table 3. Variation of $-\theta'(0)$ for some values of A^*, M and N_r when $Pr = 0.5 = S, S_f = 0.0 = S_T$.

A^*	M	Nr	$-\theta'(0)$
0.4	1.0	0.2	0.69411
0.8			0.80061
1.5			0.94861
0.3	1.2		0.64979
	1.4		0.63665
	2.5		0.57780
	1.0	0.1	0.71902
		0.3	0.61683
		0.5	0.54402

Table 4. Values of skin friction coefficient $\frac{1}{2}C_f Re_x^{1/2}$ and $-\theta'(0)$ for the parameters A^*, M, S and S_f when $Pr = 1.0, N_r = 0.2$ and $S_T = 0.1$.

M	S	S_f	A^*	$-\frac{1}{2}C_f Re_x^{1/2}$	$-\theta'(0)$
0.0	1.0	1.0	0.2	0.580873	0.724131
0.5				0.601575	0.715271
1.0				0.645009	0.697184
1.0	0.0	1.0	0.2	0.557754	0.460126
	0.2			0.575633	0.501501
	0.7			0.619717	0.621022
1.0	0.5	0.0	0.2	1.733191	0.695134
		1.0		0.602285	0.571204
		5.0		0.175027	0.491062
1.0	0.5	1.0	0.0	0.593809	0.516683
			0.3	0.606342	0.595319
			0.6	0.617821	0.655138

Table 5. Values of $-\theta'(0)$ for some values of Pr, N_r and S_T when $A^* = 0.2, S = 0.5, S_f = 1.0$.

Pr	Nr	S_T	$-\theta'(0)$

5.0	0.2	0.5	0.455178
7.2			0.573501
10.0			0.636947
7.2	0.0	0.5	0.709564
	0.3		0.607788
	0.6		0.614107
1.0	0.2	0.0	0.934592
		1.0	0.483096
		2.0	0.325735

5. SUMMARY AND NOVELTY OF ARTICLE

Current article examined mixed convection flow with velocity and temperature slips, transverse magnetic field and thermal radiation effects over a permeable elongated sheet. Computational analysis is carried out by means of unconditionally stable Keller-Box method. Graphical and tabulated results lead to the following notable findings.

- Transverse magnetic field resists fluid flow.
- The effects of M, Pr, S_T, S_f and A^*on $f'(\eta)$ are similar in a qualitative sense whereas an opposite trend is witness for λ and N_r.
- Thermal boundary layer is a decreasing function of λ, A^*, Pr and S_T.
- Influence of M, N_r and S_f on the temperature θ are opposite.
- M, S and A^* enhance Skin friction coefficient.
- Nusselt number is an increasing function of Pr. However, reverse trend is observed for N_r and S_T.
- Present analysis overlaps with existing results in literature in a limiting sense.
- Application of present analysis is useful in plastic films, polymer extrusion, glass fiber, metallurgical processes and metal spinning.

Nomenclature

x, y	Coordinate axes
u, v	Velocity components
$B(t)$	Time dependent magnetic field
ν	Kinematic viscosity
ρ	Density of fluid
σ	Electric conductivity
C_p	Specific heat
k	Thermal conductivity
q_w	Radiative heat flux
T, T_∞	Fluid temperature and ambient temperatures respectively
σ^*	Stefan-Boltzmann constant

k^*	Mean absorption coefficient
a, b, c	Constants
S	Suction / Injection parameter
A^*	Unsteadiness parameter
M	Hartman number
f, g	Dimensionless x and y components of velocity
Pr	Prandtl number
N_r	Radiation parameter
λ	Mixed convection parameter
G_r	Grashof number
S_f	Velocity slip factor
S_T	Thermal slip factor
η	Dimensionless space variable
θ	Dimensionless temperature

Subscripts

w	Wall conditions
∞	Conditions at infinity

REFERENCES

[1] Sakiadis, B. C., Boundary layer behaviour on continuous solid surface, *AIChE J*. 7 (1961), pp8-26.

[2] Bidin, B,. and Nazar, R., Numerical solution of the boundary layer flow over an exponentially stretching sheet with thermal radiation, *Eur. J. Sci. Res.*, 33 (2009),pp710-717.

[3] Akbar, N. S., et al., Numerical solutions of Magneto hydrodynamic boundary layer flow of tangent hyperbolic fluid towards a stretching sheet, *Indian J. Phys.*, 87 (2013), pp 1121-1124.

[4] Hayat, T., et al., Impact of Cattaneo-Christov heat flux in the flow over a stretching sheet with variable thickness, *AIP Advances,* 5 (2015), pp 087159.

[5] Attia, H. A., Steady flow over a rotating disk in porous medium with heat transfer, *Nonlinear Anal.: Modelling Control,* 14 (2009), pp 21-26.

[6] Rashidi, M. M., et al., Entropy generation in steady MHD flow due to a rotating porous disk in a nanofluid, *Int. J. Heat Mass Transfer,* 62(2013),pp 515-525.

[7] Manjunatha, P. T., et al., Thermal analysis of conducting dusty fluid flow in a porous medium over a stretching cylinder in the presence of non-uniform source/sink, *Int. J. Mech. Materials Eng.*, 1 (2014), pp 1-13.

[8] Acharya, M., et al., Effect of chemical and thermal diffusion with Hall current on unsteady hydro magnetic flow near an infinite vertical porous plate, *Phys. D. Appl. Phys.*, 28

(1995),pp 2455-2464.
[9] Gawin, D., et al., Coupled heat, water and gas flow in deformable porous media, *Int. J. Num. Methods Fluids*, 20 (1995), pp 969-987.
[10] Hayat, T., et al., Unsteady periodic flows lows of a magneto hydrodynamic fluid due to noncoxial rotations of a porous disk and a fluid at infinity, *Math. Computer Modelling*, 40 (2004), pp 173-179.
[11] Das, S. S., et al., Numerical solution of mass transfer effects on unsteady flow past an accelerated vertical porous plate with suction, *Bullet Malays. Math. Sci. Soc.*, 29 (2006), pp 33-42.
[12] Hameed, M. and Nadeem, S., Unsteady MHD flow of a non-Newtonian fluid on a porous plate, *J. Math. Anal. App.*, 325 (2007), pp 724-733.
[13] Das, S. S., et al., Unsteady hydro magnetic convective flow past an infinite vertical porous flat plate in a porous medium, *Int. J. Energy Environment*, 3 (2012), pp 109-118.
[14] Nadeem, S., et al., MHD three dimensional Casson flow past a porous linearly stretching sheet, *Alexandria Eng. J.*, 52(2013), pp 577--582.
[15] Saxena, P. and Agarwal, M., Unsteady flow of a dusty fluid between two parallel plates bounded above by porous medium, *Int. J. Engineering, Sci. Tech.*, 6 (2014), pp 27-33.
[16] Sharma, G. K., et al. Unsteady flow through porous media past on moving vertical plate with variable temperature in the presence of inclined magnetic field, *Int. J. Innovative Technol. Research*, 4 (2006), pp 2784-2788.
[17] Elbashbeshy, E. M. A. and Aldawody, D. A., Effects of thermal radiation and magnetic field on unsteady mixed convection flow and heat transfer over a porous stretching surface, *Int. J. Nonlinear Sci.*, 9 (2010), pp 448-454.
[18] Hayat, T., et al., Effects of radiation and magnetic field on the mixed convection stagnation-point flow over a vertical stretching sheet in a porous medium, *Int. J. Heat Mass Transfer*, 53 (2010),pp 466-474.
[19] Rashidi, M. M. and Abbasbandy, S., Analytic approximate solutions for heat transfer of a micropolar fluid through a porous medium with radiation, *Commun. Nonlinear Sci. Numerical Simul..*, 16 (2011) pp 1874-1889.
[20] Uwanta, I. J. and Hamza, M. M., Effect of suction/injection on unsteady hydro magnetic convective flow of reactive viscous fluid between vertical porous plates with thermal diffusion, *Int. Scholarly Research Notices*,2014 (2014),pp980270.
[21] Kandasamy, R and Muhaimin, I., Impact of thermal stratification on unsteady Hiemenznondarcy copper nanofluid flow over a porous wedge in the presence of magnetic field due to solar radiation (green) energy, *Chemical Process Eng. Research*, 36 (2015),pp22250913.
[22] Shirvan, K. M., et al., Enhancement of heat transfer and heat exchanger effectiveness in a double pipe heat exchanger filled with porous media: Numerical simulation and sensitivity analysis of turbulent fluid flow, *Appl. Thermal Eng.*, 109 (2016),pp 761-774.
[23] Turkyilmazoglu, M., Mixed convection flow of magneto hydrodynamic micropolar fluid due to a porous heated/cooled deformable plate: Exact solutions, *Int. J. Heat and Mass Transfer*, 106 (2017), pp 127–134.
[24] Turkyilmazoglu, M., Equivalences and correspondences between the deforming body induced flow and heat in two-three dimensions, *AIP Physics of Fluids*, 28 (2016), pp 043102-1-10.
[25] Turkyilmazoglu, M., Magnetic field and slip effects on the flow and heat transfer of stagnation point Jeffrey fluid over deformable surfaces, *Zeitschrift für Naturforschung A*, 71 (2016), pp 549-556.
[26] Wang, C. Y., Flow due to a stretching boundary with partial slip - an exact solution of the Navier-Stokes equations, *Chem. Eng. Sci.*,57 (2002), pp 3745-3747.

[27] Ishak, A., et al., Heat transfer over an unsteady stretching permeable surface with prescribed wall temperature, *Nonlin. Analysis: Real World Appl.*, 10 (2009), pp 2909-2913.